Franka Ennen, Susanne Boye, Albena Lederer, Mihaela Cernescu, Hartmut Komber, Bernhard Brutschy, Brigitte Voit, Dietmar Appelhans

Biohybrid structures consisting of biotinylated glycodendrimers and proteins: influence of the biotin ligand's number and chemical nature on the biotin–avidin conjugation

Erstveröffentlichung in / First published in:
Polymer Chemistry. 2014, 5(4), S. 1323–1339 [Zugriff am: 04.11.2019]. Royal Society of Chemistry. ISSN 1759-9962.

DOI: https://doi.org/10.1039/c3py01152f

Polymer Chemistry

PAPER

View Article Online
View Journal | View Issue

Cite this: *Polym. Chem.*, 2014, **5**, 1323

Biohybrid structures consisting of biotinylated glycodendrimers and proteins: influence of the biotin ligand's number and chemical nature on the biotin–avidin conjugation†

Franka Ennen,[ab] Susanne Boye,[a] Albena Lederer,[ab] Mihaela Cernescu,[c] Hartmut Komber,[a] Bernhard Brutschy,[c] Brigitte Voit*[ab] and Dietmar Appelhans*[a]

Received 29th August 2013
Accepted 16th October 2013

DOI: 10.1039/c3py01152f

www.rsc.org/polymers

We present the bioconjugation of avidin as a central and/or bridging building block with mono-, bi- and tetravalent biotinylated glycodendrimers to fabricate defined supramolecular nanostructures for future (bio)medical applications. For this purpose mono-, bi- and tetravalent biotinylated glycodendrimers, decorated with short alkyl-linked or long PEG-linked biotin ligands, were synthesized and characterized by NMR, IR and mass spectrometry and HABA displacement assay. Various techniques (UV/Vis, DLS, TEM, LILBID-MS and AF4) were used in order to obtain information about the structural properties of different conjugates of avidin and mono-, bi- and tetravalent biotinylated glycodendrimers. The biotin ligand's spacer length, its chemical structure and the degree of biotin functionalization are essential parameters in the formation of nanostructures with avidin having a controlled composition and size dimension up to 100 nm. Biohybrid structures with avidin as a central unit require monovalent glycodendrimers with PEG-linked biotin, while bi- and tetravalent glycodendrimers with short alkyl-linked biotin ligands are more efficient than their counterparts with longer PEG–biotin ligands in the fabrication of defined biohybrid structures (∅ up to 100 nm) with avidin as a bridging unit. The most dominating key issue, combined with other conjugation issues, is the optimal ligand–receptor stoichiometry to fabricate biohybrid structures with diameter of <20, <30 or up to 100 nm.

Introduction

The design of versatile nanostructured biohybrid materials has gained increasing attention over the past decades due to their potentially extraordinary and synergetic properties and functions. The combination of components of synthetic and natural origins allows an applicability going far beyond the biomedical field including diverse matters such as bio-sensors, artificial enzymes, light harvesting systems, photonics and nanoelectronic devices. Thus, the formation of higher ordered molecularly organized structures has been explored widely. These artificial supramolecular structures include solid core nanoparticles, as well as linear and perfectly branched polymeric materials.[1–8]

Along with other bioconjugation techniques the avidin–biotin interaction has received great interest due to its tremendously high, non-covalent bonding strength ($K_d = 10^{-15}$ M) making it a convenient conjugation technique.[9]

Recently scientists have developed approaches to fabricate dendrimer based sensory and enzymatic biohybrid structures, but mainly attached to solid surfaces, combining the advantages of dendritic structures and the strongest known non-covalent bond.[10–18]

The development of intravenous formulations and the control of release kinetics lead to the fabrication of nanoparticles (<1 μm). Small particles (<20–30 nm) are usually eliminated by renal excretion after administration. Since nanoparticles can escape the circulation through so called fenestrations of the endothelial barrier, the optimal size for drug delivery applications in cancer research is between 70 and 200 nm and highlights the vital interest in controlled sizes of fabricated biohybrid structures for applications in imaging and drug and/or gene delivery.[19]

However, it had been found that the conjugation of polymeric particles to avidin can enhance accumulation in tumour tissue mediated through the EPR effect due to increased molecular weights of the associates.[20,21] Moreover, avidin has also the ability

[a]*Leibniz Institute of Polymer Research Dresden, Hohe Str. 6, 01069 Dresden, Germany. E-mail: applhans@ipfdd.de; voit@ipfdd.de*

[b]*Technische Universität Dresden, 01062 Dresden, Germany*

[c]*Institute for Physical and Theoretical Chemistry, Johann-Wolfgang-Goethe University, Max-von-Laue-Str. 7, 60438 Frankfurt/Main, Germany*

† Electronic supplementary information (ESI) available: Additional information is provided in tables and figures for NMR, LILBID-MS, DLS, UV-Vis, HABA displacement assay and TEM. See DOI: 10.1039c3py01152f

of binding to different lectins expressed on different cancer cell surfaces.[13,22–25] This potentially makes avidin combined with polymeric particles a versatile building block especially in cancer research through both passive and active targeting. A recent study showed in an impressive manner, how a biotin-functionalized dendron in a dendritic multi-domain delivery system can enhance the cellular uptake of two therapeutic proteins in mammalian cells by using streptavidin as central core units in such a delivery system.[26] Moreover, the avidin's very high avidity toward biotin and its lack of harmful immunogenicity[27] lead to a very high research activity conducted on avidin as a carrier for cancer drug delivery.

On the other hand dendrimers have been proposed as ideal candidates as supramolecular building blocks, since they are structured by central core, branching units and high numbers of terminal functional groups. Their unique and perfect structure offers various interaction properties (*e.g.* encapsulation of drugs or stabilisation of nanoparticles), whereas their peripheral functional groups tailor their solubility and chemical behaviour.[28,29] The high numbers of surface groups can be used to introduce a variety of functional groups that can work as biocompatibility mediators, enhance the blood circulation times in drug or gene delivery vesicles (*e.g.* PEG terminated or OH group terminated dendrimers),[5,30] or work as recognition moieties. Moreover, peripheral functional groups which are considered as randomly distributed but maximally separated substituents[31–34] (*e.g.* alkyl or aromatic units) can act in the outer shell of dendrimers to initiate uncontrolled/controlled self-assembly processes. In this context certain studies in solution revealed a significant dependence of the biotinylated materials' properties on the final structure of the self-assembled nanostructures.[35–38] It seems not always appropriately addressable[14,15,35] to get sufficient information about the properties of such supramolecular structures in solution. With respect to pivotal properties (*e.g.* shape, size, morphology or molar masses) of those nanostructures, the necessity for a comprehensive and thorough characterization has been emphasized by various researchers recently.[6,19,30,39] This led us to the conclusion that the self-assembly of avidin with mono-, bi- and tetravalent biotinylated dendrimers in solution (Fig. 1) still poses open questions with respect to homogeneity of the samples, controlled sizes and specific functions, especially with regard to their use as defined supramolecular entities in biomedical applications such as gene and drug delivery.

This report presents a comprehensive study of the interaction of avidin with high generation (4th) dendrimers possessing biotin ligands with varied spacer lengths, different biotinylation degrees in particular 1, 2 and 4 and an oligosaccharide modified shell, which is known to possess a high biocompatibility and a neutral surface.[40,41] Thus, the successful formation of different biohybrid associates was identified by a variety of analytical tools (HABA titration experiments, DLS and TEM), where simultaneous binding events between avidin and biotinylated macromolecules were tested. The variation in the avidin–biotin conjugations should clarify whether avidin can be used as a central or bridging building block. Here, we generally investigated the pure conjugation solutions for exhibiting the potential use of various biotinylated poly(propylene imine) (PPI) glycodendrimers (**bGD**; Fig. 2) in the fabrication of defined biohybrid structures. A first glance of possible biohybrid structures using mono- and bivalent **bGD** is highlighted in Fig. 1. Moreover, the investigation through novel techniques such as asymmetrical flow field flow fractionation (AF4) and laser-induced liquid bead ionization/desorption mass spectrometry (LILBID MS) revealed further important features of the final compositions of those biohybrid structures. This study may not only elucidate the formation of biohybrid structures between avidin and biotinylated PPI glycodendrimers in the conjugation solution, but also will give deeper insight into these supramolecular (bio)polymeric structures from a general point of view.

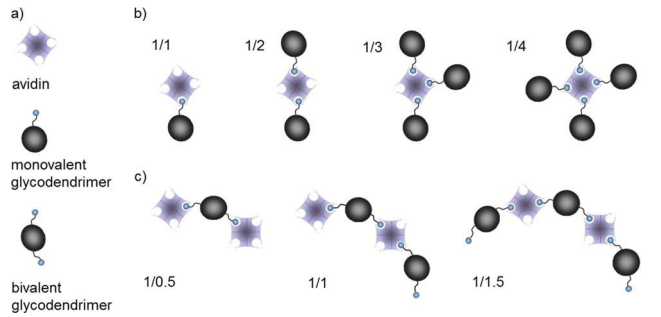

Fig. 1 Possible biohybrid structures from the theoretical point of view when conjugating monovalent (a) and bivalent (b) biotinylated glycodendrimers with avidin in defined molar ratios. Those supramolecular structures, obtained here in this study, will be directly analysed in conjugation solution.

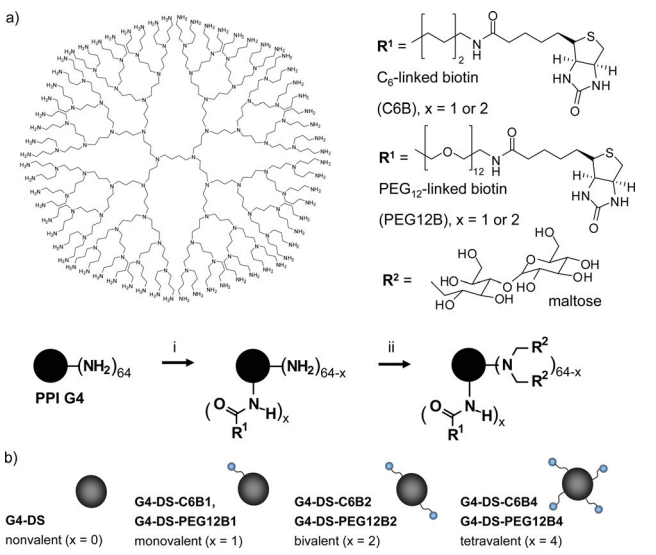

Fig. 2 (a) Synthesis of biotinylated glycodendrimers G4-DS-C6B*x* and G4-DS-PEG12B*x*, $x = 1$, 2 and 4: (i) conversion of PPI-G4 with a biotin ligand and BOP in DMSO at room temperature for 2 days; biotin ligand: biotinyl-6-aminocaproic acid (C6B) or HOOC-PEG_{12}-biotin (PEG12B); (ii) reductive amination of the precursor with a ratio of NH_2/maltose/BH_3·Pyr of 1/20/20 in sodium borate solution at 50 °C for 7 days followed by dialysis in distilled water; the details of the molar ratios can be seen in Table 2; (b) overview of final compounds.

Table 1 Characteristics of biotinylated glycodendrimers and their precursors; Mal = maltose

Biotinylated glycodendrimer (**bGD**)	Ligand[a]	Biotin determination	LILBID-MS		Precursor	
		Number of ligands[b]	$M_{observed}$ in g mol^{-1}	Number of Mal		M in g mol^{-1}
G4-DS	—	0	46 900[c]	122 (128)[e]	**G4**	7168[g]
G4-DS-C6B1	**C6B** (1)	1.1	46 000[c]	118 (126)[e]	**G4-C6B1**	7500[h]
G4-DS-C6B2	**C6B** (2)	2.1	46 100[c]	117 (124)[e]	**G4-C6B2**	7850[h]
G4-DS-C6B4	**C6B** (4)	3.6	47 650[c]	120 (120)[e]	**G4-C6B4**	8500[h]
G4-DS-PEG12B1	**PEG12B** (1)	1.1	45 900[c]	116 (126)[e]	**G4-PEG12B1**	8000[h]
G4-DS-PEG12B2	**PEG12B** (2)	2.0	45 700[c]	113 (124)[e]	**G4-PEG12B2**	8820[h]
G4-DS-PEG12B4	**PEG12B** (4)	4.2	43 750[d]	102 (120)[f]	**G4-PEG12B4**	10 500[h]

[a] Number in brackets represents the theoretical number of biotin ligands attached to the corresponding G4 scaffolds. [b] Number of biotin ligands was determined by the avidin-4′-hydroxyazobenzene-2-carboxylic acid (HABA) complex using a specific activity of avidin of 13.6 units per mg. [c] Determined by LILBID MS. [d] Calculated by ^{1}H NMR based on the number of biotin groups (*cf. b*). [e] Number of maltose units determined through LILBID-MS. [f] M is used for estimating the number of maltose units of the glycodendrimers as described in the literature.[41] [g] M was determined by MALDI-TOF mass spectrometry. Results from mass determination confirm the molar mass data of G4 obtained by the company SyMOChem (Eindhoven, The Netherlands). [h] M was determined by M_n of PPI-G4 and the degree of biotin substitution.

Results and discussion

Synthesis and characterization of biotinylated glycodendrimers

The general strategy for the synthesis of biotinylated glycodendrimers with a dense maltose shell is shown in Fig. 2. In particular, the following biotinylated 4th generation glycodendrimers‡ with a dense maltose shell (**G4-DS**) were synthesized, characterized (Table 1) and used in our study: non-biotinylated **G4-DS** as a reference, **G4-DS-C6B1** mono-functionalized with a C6-linked biotin, **G4-DS-C6B2** di-functionalized with a C6-linked biotin, **G4-DS-C6B4** tetra-functionalized with a C6-linked biotin, **G4-DS-PEG12B1** mono-functionalized with a PEG12-linked biotin, **G4-DS-PEG12B2** di-functionalized with a PEG12-linked biotin and **G4-DS-PEG12B4** tetra-functionalized with a PEG12-linked biotin.

To functionalize the PPI-G4 scaffold (64 peripheral amino groups) the dendrimers were converted either with 6-(*N*-biotinylamino)caproic acid (**C6B**) or biotin-PEG$_{12}$-COOH (**PEG12B**), benzotriazole-1-yl-oxy-tris-(dimethylamino)-phosphonium hexafluorophosphate (**BOP**) and an excess of triethylamine in the first step. In the second step of the synthesis the remaining primary amino groups were preferentially disubstituted with maltose using a 20 fold excess of maltose monohydrate in borate buffer in the presence of $BH_3 \cdot Pyr$ in a reductive amination step. Biotinylated precursors and glycodendrimers were characterized and identified by NMR spectroscopy, IR spectroscopy, mass spectrometry and HABA displacement assay.

Key characteristic steps have been the biotin ligand coupling on the PPI dendrimer surface and the determination of the average number of biotin ligands coupled to each glycodendrimer, while the final molar mass of biotinylated glycodendrimers was easily available through LILBID-MS (Table 1).

Both the precursors and the glycodendrimers were characterized by ^{1}H NMR spectroscopy. Exemplarily, Fig. 3a depicts the spectrum of precursor **G4-PEG12B2** with signal assignment. A doublet at 2.75 ppm indicates that a small amount of PPI-bonded hexamethylphosphoramide is formed in a side-reaction

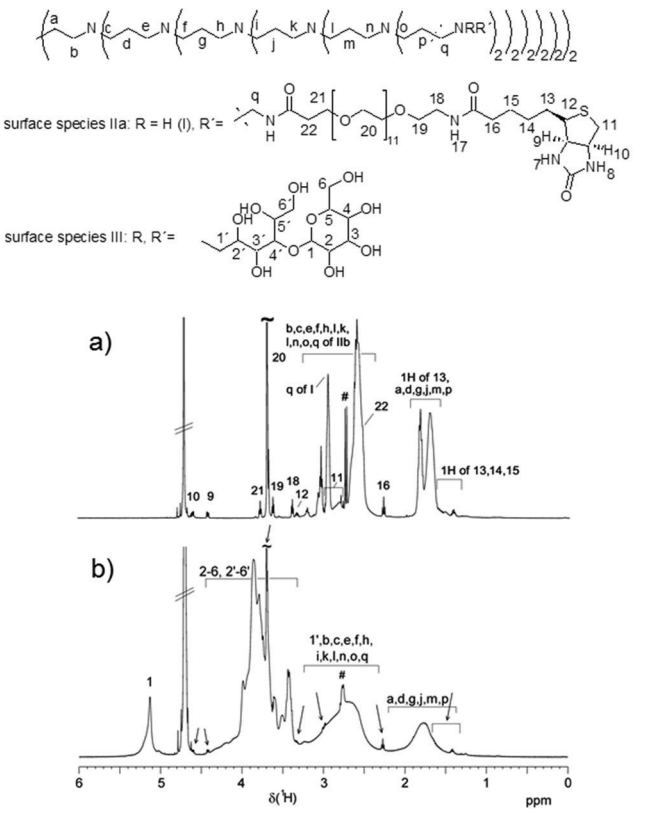

Fig. 3 ^{1}H NMR spectrum (a) of **G4-PEG12B2** and (b) of **G4-DS-PEG12B2** (solvent: D_2O). The signals of the biotin ligand **PEG12B** and of the PPI-G4 core are assigned in (a). Maltosylation results in additional broad signals which are shown in (b). Arrows point to ligand signals well observable also after maltosylation (# hexamethylphosphoramide derivative).

‡ Following suggestion from D.A. Tomalia and M. Rookmaker for "Poly(propyleneimine) Dendrimers" in *Polymer Data Handbook*,[42] the nomenclature for Tomalia-type PAMAM dendrimers and other can be adopted also for PPI dendrimers. This means that the commercially available 5th generation PPI dendrimer, used here in this study, is a 4th generation.

most probably due to the rather large excess of **BOP** applied for complete conversion of the ligand. A correct calculation of the number of ligands from signal integrals is hampered by signal overlap of the ligand and PPI core signals of the precursors. With the reasonable assumption that one equivalent of the ligand is completely converted in the presence of a 64-fold excess of amino end groups, a comparison of the spectra using PPI signals as an intensity reference (in Fig. ESI-3†) confirms the substitution of the biotin ligands in an approximately 1 : 1 and 1 : 2 ratio for -B1 and -B2 precursors, respectively. After maltosylation only few but characteristic ligand signals can be well observed (Fig. 3b) proving the functionalization of the glycodendrimer **G4-DS-PEG12B2** also after this reaction step.

Additionally to the NMR study, the number of bound biotin ligands on each glycodendrimer was determined by HABA displacement titration experiments according to the literature[43] (Fig. 4). The average number of bound biotin ligands on the dendritic glycosurface is summarized in Table 1. In most cases the theoretically required number of biotin ligands coupled to each glycodendrimer was evaluated. Interestingly, non-biotinylated **G4-DS** shows also a replacement of the azo dye, but the lack of a clear endpoint indicates no specific interaction and a dissociation constant in the range of 10^{-9} to 10^{-6} M.[7] In context of the latter, it has been shown that only a pretreatment of (strept-)avidin with a high excess of pure maltose leads to a significant inhibition of the (strept-)avidin–biotin interaction where an unexpected interaction of maltose units in the binding pockets in (strep-)avidin can be assumed.[44] In our study, we can probably exclude such a binding event between maltose units and binding pockets of avidin due to the high amount of chemically attached maltose units on the dendritic PPI scaffold.

Knowing the average number of biotin ligands on each glycodendrimer surface and molar mass of biotinylated glycodendrimers we were able to start our study for fabricating and characterizing the various biohybrid structures mentioned below.

Interaction of mono- and bivalent biotinylated glycodendrimers with avidin

The coupling of the biotinylated glycodendrimers (**bGD**) to avidin as a central and bridging building block led to nanometer-sized biohybrid structures with potential functionalities. Their schematic illustration is presented in Fig. 1. For the DLS study of the formed biohybrid structures avidin was converted with stoichiometric amounts of the (non-)biotinylated glycodendrimers: **G4-DS** (1 and 3 equivalents (eq.)) (Fig. ESI-8†), **G4-DS-PEG12B1** (1–4 eq.) and **G4-DS-C6B1** (1–4 eq.) as well as **G4-DS-PEG12B2** (0.5, 1 or 1.5 eq.) and **G4-DS-C6B2** (0.5, 1 or 1.5 eq.) in the presence of 1 equivalent avidin (Fig. 5 and Table 2). Generally, all conjugation solutions for the used **C6B1**, **C6B2**, **C6B4**, **PEG12B1**, **PEG12B2** and **PEG12B4** ligands in this study have a total mass concentration of about 0.6–0.7 mg mL^{-1} and no precipitation was observed in all cases. In the case of the bi- and tetravalent **bGD** we aimed to probe the conjugation potential of the **bGD** when avidin is in excess, avidin and **bGD** are equimolar or **bGD** is in excess.

Two general points can be identified after the formation of the various biohybrid structures: increasing the stoichiometric amount of **bGD** against avidin obviously results in growth of the final biohybrid structures (Fig. 5, left panel). This growth is accompanied by a decrease in the absorbance of complexed HABA in the binding pockets of avidin at 500 nm in the HABA displacement assays (Fig. 5, middle panel). Avidin and almost all **bGDs** possess diameters of about 5–6 nm as the starting point for evaluating the biohybrid structures.

Considering the biohybrid structure with avidin as a potential central building block (Fig. 5a) with monovalent **bGD G4-DS-C6B1**, a general decrease in the A_{500nm} absorbance can be observed for all avidin–**G4-DS-C6B1** associates with molar ratios from 1/1 up to 1/4. Contrary to that the DLS data show only increasing sizes up to a ratio of 1/3 (Fig. 5a, molar ratio 1/1 to 1/4; ∅ 12 nm determined as peak maximum (volume (vol)%) after 24 h for the 1/3 and 1/4 ratios by DLS). For this conjugation between avidin and increasing numbers of the biotin ligand **C6B**, the size growth to larger biohybrid structures is obviously hampered by the shielding properties of the dense maltose shell where the biotin ligand **C6B** is surrounded by larger maltose units in the outer shell of **G4-DS-C6B1**. This means that **C6B** is too short and not apparent in a sufficient amount in the desired conjugation step to overcome the hampering effect of the dense maltose shell. Moreover, the required length of 0.9 nm (ref. 45) of the biotin ligand **C6B** in **G4-DS-C6B1** to reach the avidin binding site is not apparent. In contrast to that a sufficient spacer length is given in the case of the biotin ligand **PEG12B** in

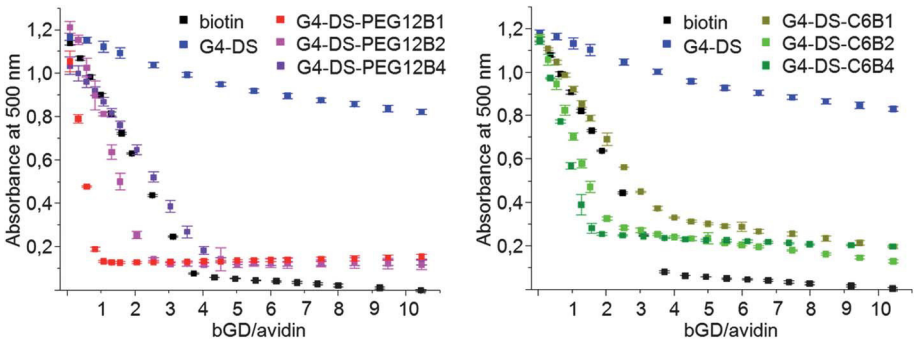

Fig. 4 HABA displacement assay: titration of a preformed avidin–HABA complex with left panel: **G4-DS-PEG12Bx** ($x_{theoretical}$ = 1, 2 and 4) and right panel: **G4-DS-C6Bx** ($x_{theoretical}$ = 1, 2 and 4) as well as **G4-DS** and biotin as references.

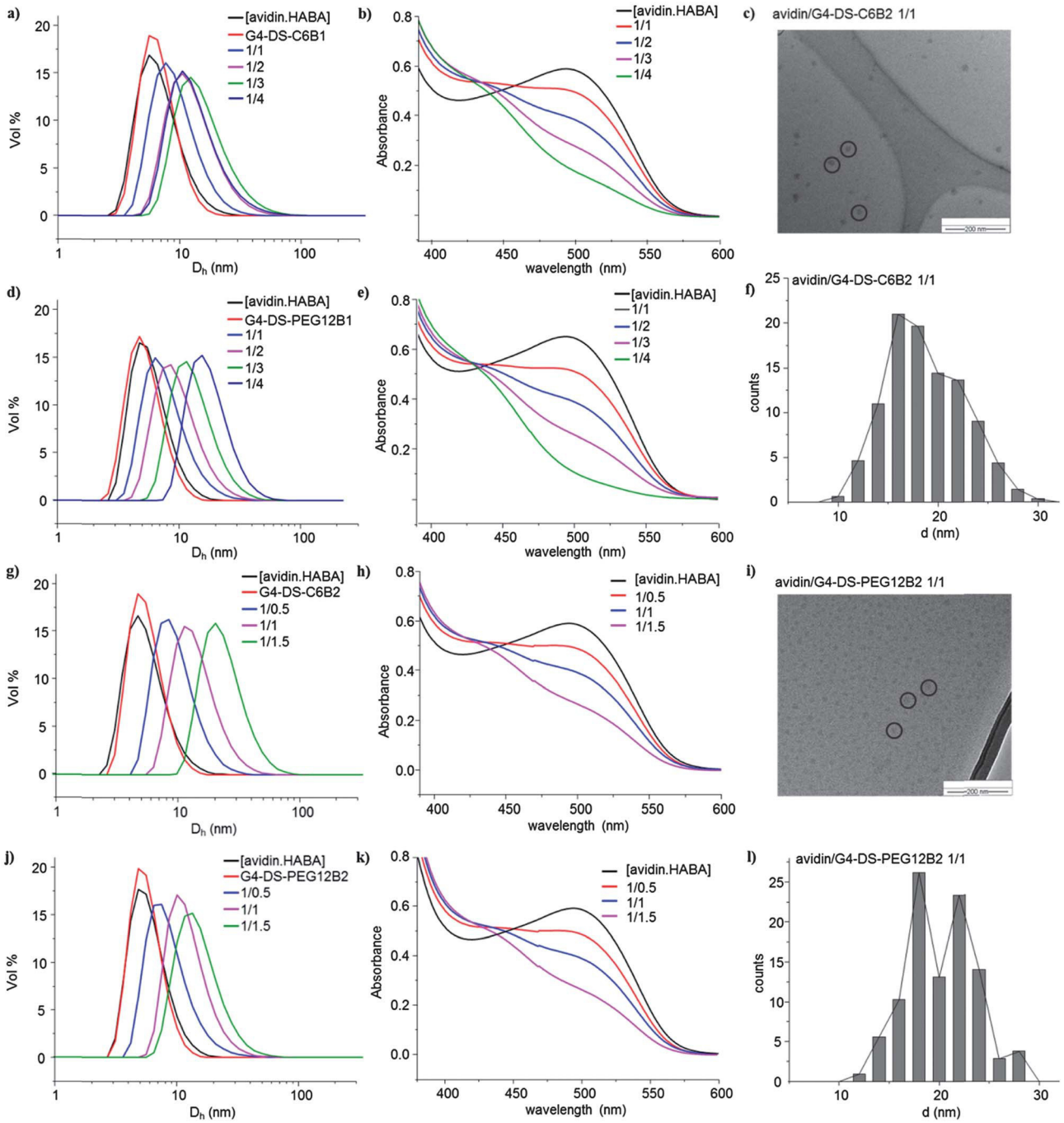

Fig. 5 Left panel: DLS results of the conversions of avidin with biotinylated glycodendrimers, middle panel: corresponding HABA displacement assay results, right panel: (c) TEM images of avidin and **G4-DS-C6B2** 1/1, (f) TEM size measurements: particle size distribution of avidin–**G4-DS-C6B2** 1/1; (i) TEM image of avidin and **G4-DS-PEG12B2** 1/1, (l) TEM size measurements: particle size distribution of avidin–**G4-DS-PEG12B2** 1/1.

G4-DS-PEG12B1 allowing the compensation of the shielding effect of the dense maltose shell. This leads to a homogeneous increase in size with increasing amounts of the **G4-DS-PEG12B1** sample against avidin (molar ratio 1/1 to 1/4, Fig. 5d – ∅ 18 nm determined as peak maximum (volume (vol)%) after 24 h for the 1/4 ratio by DLS).

The next step was to consider the biohybrid structures with avidin as a potential bridging unit (Fig. 1b), which requires functionalization with at least 2 biotin ligands in **bGD** (**G4-DS-C6B2** and **G4-DS-PEG12B2**; Fig. 5g and j). This higher functionalization should naturally increase the probability of occupied avidin binding sites by both biotin ligands, **C6B** and **PEG12B**. For example, a molar ratio of 1/1 between avidin and **G4-DS-C6B2** (Fig. 5g) results in a larger biohybrid structure size in comparison with those of **G4-DS-C6B1** (Fig. 5a). Indeed, the conversion of avidin with **G4-DS-C6B2** (Fig. 5g) or **G4-DS-PEG12B2** (Fig. 5j) shows in both cases an increase in size upon addition of increasing amounts of **bGD**. The avidin–**G4-DS-C6B2** associates

Table 2 Overview of mean diameters (*d*) of avidin, **bGDs** and bioconjugates measured after 1 day taken from the volume distribution

Sample name	PdI	*d* (V%)/nm	V%
Avidin[a]	0.27	7.9	100
G4-DS-C6B1[a]	0.338	5.9	100
1/1	0.235	8.1	100
1/2	0.24	11.1	100
1/3	0.228	13.3	100
1/4	0.273	11.6	100
G4-DS-C6B2[a]	0.34	6.1	100
1/0.5	0.261	9.6	100
1/1	0.216	14.6	100
1/1.5	0.169	28.4	100
G4-DS-PEG12B1[a]	0.355	5.6	100
1/1	0.224	9.1	100
1/2	0.221	10.7	100
1/3	0.204	13.1	100
1/4	0.165	17.9	100
G4-DS-PEG12B2[a]	0.375	6.0	100
1/0.5	0.341	9.9	100
1/1	0.222	12.7	100
1/1.5	0.18	16.7	100
G4-DS-C6B4[a]	0.284	5.6	100
1/0.5	0.2	30.2	100
1/1	0.138	48.6	100
1/1.5	0.231	20.0	100
G4-DS-PEG12B4[a]	0.43	6.1	100
1/0.5	0.16	40.5	100
1/1	0.184	39.9	100
1/1.5	0.246	20.9	100

[a] Samples were only measured after 1 day.

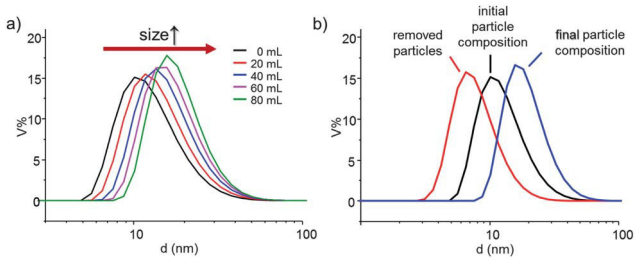

Fig. 6 Measured diameters of supramolecular organizations of avidin with **G4-DS-PEG12B2** 1/1 purified through hollow fibre filtration. (a) Increasing resulting diameters with increasing purification time; (b) comparison of the diameter of the removed particles (∅ 8 nm, DLS volume distribution), the initial compositions (∅ 13 nm, DLS volume distribution) and the resulting particle composition (∅ 20 nm, DLS volume distribution).

show diameters up to ∅ 28 nm determined as peak maximum (volume (vol)%) after 24 h for the 1/1.5 ratio by DLS (Fig. 5g – molar ratio 1/0.5; 1/1; 1/1.5). In contrast the **G4-DS-PEG12B2**-based associates provide diameters up to ∅ 17 nm after 24 h (Fig. 5j, DLS – molar ratio 1/0.5; 1/1; 1/1.5 with increasing **G4-DS-PEG12B2**).

This surprising result from the **G4-DS-PEG12B2** conjugation step can be explained by interfering interactions of the PEG chains between **G4-DS-PEG12B2** macromolecules as well as undesired non-specific interactions of PEG chains with the glycoprotein avidin during the avidin–biotin conjugation. Although PEG is generally known for its protein repellent properties, it has been reported that PEG does interact with certain proteins such as mucin,[46] lysozyme[47,48] or bovine serum albumin.[48] However, either repellent or non-repellent interactions of PEG with proteins are critically dependent on various factors such as the amount of PEG chains on the surface, their length, the protein conformation properties or the presence of certain amino acids.[37,38,46,47,49]

To further clarify the efficiency of **PEG12B2** ligands the non-homogenous solution was exemplarily filtered by the hollow fibre filtration method to separate non-conjugated **bGD** from biohybrid structures after the conjugation step between **G4-DS-PEG12B2** and avidin with 1/1 molar ratio (Fig. 6). After this purification process the average diameter of these dendritic supramolecular structures is about 20 nm, while the non-homogenous solution after the conjugation process shows an average diameter of about 13 nm for the conjugates (Table 2). This additional purification step impressively shows us that a successful separation of non-conjugated **bGD** and avidin from the desired biohybrid structures is possible. This first purification result offers us the chance in the future to obtain purer biohybrid structures more suitable for biomedical applications.

Analysing the results from the TEM images of the various biohybrid structures of **PEG12B1** with 1/1 and 1/3 molar ratios (Fig. ESI-9†), **C6B2** with 1/1 molar ratio (Fig. 5c and f) and **PEG12B2** with 1/1 molar ratio (Fig. 5i and l), one can recognize two tendencies: firstly, **PEG12B1** biohybrid structures strongly tend to aggregate into spherical particles with diameters between 25 and 40 nm. In contrast to that, biohybrid structures obtained from **G4-DS-C6B2** and **G4-DS-PEG12B2** with 1/1 molar ratio to avidin outline diameters in the range of 18 and 25 nm. On the one hand one has to take into account that the TEM images show particles in the dry state, which may be partly distorted due to the evaporation of the solvent. This lead to different kinds of aggregated (**PEG12B1**) and non-aggregated (**PEG12B2** and **C6B2**) biohybrid structures in our study. Furthermore, compared to the DLS study decreased buffer molarity and increased total concentrations were used in the TEM study in order to ensure the imaging of the supramolecular organizations. On the other hand it has to be considered that DLS size curves present certain size distribution. If there are populations present that differ only in a few nanometers in their sizes, one will measure the overlap of the sizes of these populations *e.g.* avidin and/or **bGD** and formed associates. The higher the amount of non-conjugated biotinylated glycodendrimer, the lower are the mean diameters of biohybrid structures (*e.g.* Fig. 5a and g). This point was impressively confirmed by the purification step of **G4-DS-PEG12B2** biohybrid structures with 1/1 molar ratio (Fig. 5g and 6b) allowing for the separation of non-conjugated components. Now, the final diameter of the purified biohybrid structures from the DLS study (Fig. 6) nicely

matches the average diameter obtained from the TEM study (Fig. 5l). Thus, there is a good correlation in this specific example (Fig. 5i, l and 6), while the larger detectable diameters from the DLS study in the case of **C6B2** with 1/1 molar ratio (Fig. 5g) and **PEG12B2** with 1/1 molar ratio (Fig. 5j) also preferentially match the mean diameters evaluated by the TEM study (Fig. 5f and l) when excluding the lowering effects of non-conjugated components.

The results from the DLS study have been supported by estimating the apparently bound amount of **bGD** to avidin. A linear regression of the lower part of the titration curve (*cf.* Fig. 4) and the change in absorbances in the HABA displacement assays (Fig. 5b, e, h and k) were used to determine the amount of displaced dye and the amount of bound **bGD**, respectively. The determined apparent values compared to the initial molar ratios are summarized in Table 3. It revealed that in most samples only about one half of the **bGD** are bound to avidin. This seems surprising, since avidin–biotin conjugation is characterized by a very low dissociation constant of 10^{-15} M.

The much lower binding strength of mono- and bivalent **bGD** against avidin is preferentially explainable when considering the structural properties of avidin and **bGD** and the discussed conjugation mechanism of biotin on the avidin binding sites: firstly, it is influenced by a sterical shielding effect of **bGD** (Fig. 7c) when they are coupled to the avidin binding site. This is supported by (A) the binding of about 50% of **bGD** to the avidin scaffold (Table 3) and smaller mean diameters (DLS study) influenced by non-conjugated **bGD** and (B) similar diameters of avidin and **bGD** of about 5–6 nm. For better understanding the lower binding strength of **bGD** against avidin, the structural dimensions of avidin with its binding sites are simplified,[50,51] presented in Fig. 7a. Moreover, it was shown by spin-labelled biotin derivatives that those were initially bound in a random fashion and changed slowly from a possible *cis* position to a more favoured *trans* position on the avidin binding sites (Fig. 7b).[50] This kind of rearrangement of biotin derivatives was also discussed by Kisak *et al.*[52] and Connolly *et al.*[53] Thus, it can be proposed that the conjugation mechanism for binding **bGD** on avidin binding sites takes place in the same fashion as postulated for much larger and equally sized biotin derivatives. With this in mind the formation of (larger) biohybrid structures with avidin as central and bridging units (Fig. 5) is accompanied by (A) permanently occurring association and dissociation processes with respect to *cis–trans* rearrangement of biotin derivatives on avidin binding sites (Fig. 7b), and (B) permanently apparent sterical demands of **bGD** preferentially preventing the conjugation of a third and fourth **bGD** on avidin binding sites (Fig. 7c). Finally, in the case of **G4-DS-C6B1** with 1/2, 1/3 and 1/4 molar ratios similar mean diameters between 11 and 13 nm (Table 2) can be found while an increased release of HABA molecules is observable (Table 3). This implies that even more simultaneous association–dissociation steps of **G4-DS-C6B1** against avidin take place and the resulting binding of **G4-DS-C6B1** on avidin binding sites is weak due to reasonable points (sterical demands, spacer length, *etc.*). Thus, in the 1/4 conjugation solution even more non-conjugated **bGD** and avidin, respectively, are responsible for lowering the mean diameter in comparison to 1/3 conjugation solution (Table 2).

Table 3 Summary of initial avidin–bGD stoichiometry and bound glycodendrimer in the biohybrid structure for G4-DS-C6B1, G4-DS-C6B2, G4-DS-PEG12B1, and G4-DS-PEG12B2

Avidin–**bGD**	Initial molar ratio	Bound GD[a]
Avidin–**G4-DS-C6B1**	1/1	0.49
	1/2	0.99
	1/3	1.47
	1/4	1.92
Avidin–**G4-DS-C6B2**	1/0.5	0.35
	1/1	0.53
	1/1.5	0.87
Avidin–**G4-DS-PEG12B1**	1/1	0.50
	1/2	0.97
	1/3	1.49
	1/4	2.04
Avidin–**G4-DS-PEG12B2**	1/0.5	0.31
	1/1	0.50
	1/1.5	0.75

[a] Based on the amount of HABA displaced by biotin ligands.

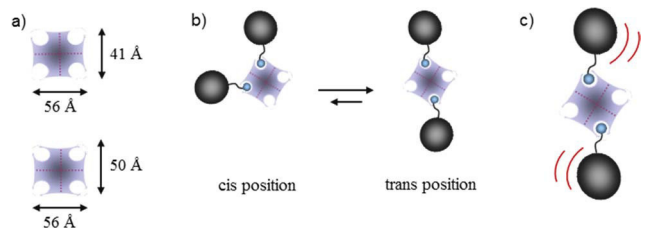

Fig. 7 (a) Structure and dimensions of avidin;[50,51] (b) assumed favoured coupling of two bGD as proposed by Sinha *et al.*;[50] (c) sterical shielding effect of the coupled glycodendrimers due to similar sizes of avidin and the bGD.

However, a lack of complete conversion of avidin with bis-biotinyl-functionalized alkanes was also reported by Green *et al.*[45] In order to further evaluate the size determining key factors for fabricating defined biohybrid structures, **bGD** with four biotin ligands **C6B** and **PEG12B** (**G4-DS-C6B4** and **G4-DS-PG12B4**) have been used to investigate their conjugation potential with avidin.

Interaction of tetravalent biotinylated glycodendrimers with avidin

While biohybrid structures with a maximal diameter of ~30 nm are available in the case of the **G4-DS-C6B2** conjugation step (Fig. 5g and Table 2), **G4-DS-C6B4** and **G4-DS-PG12B4**, possessing 4 biotin ligands, produce nanoparticles of up to 100 nm in diameter. This result was determined by using molar ratios of 1/0.5, 1/1 and 1/1.5 for fabricating avidin–**bGD** associates (Fig. 8) of different sizes along with evaluating the peak maxima by DLS (Tables 2 and 4).

One can impressively identify different conjugation behaviours of both **bGD** against avidin macromolecules mainly triggered by the type of biotin ligand. The size distributions of the

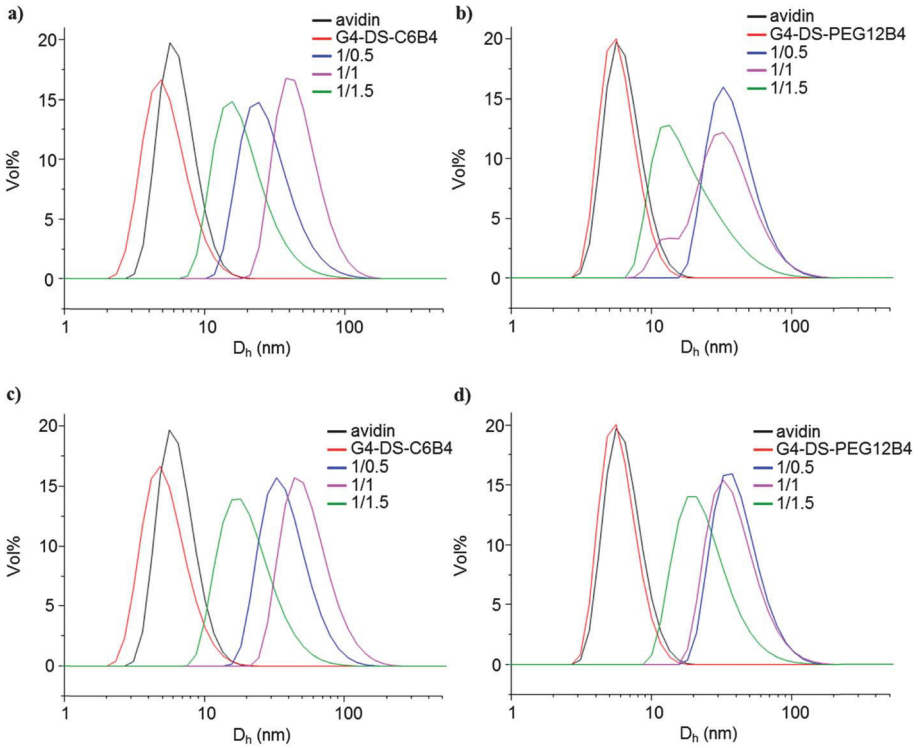

Fig. 8 DLS results of conversions of avidin with **G4-DS-C6B4** (a) after 1 day and (c) after 7 days and with **G4-DS-PEG12B4** (b) after 1 day and (d) after 7 days.

Table 4 Overview of mean diameters of avidin, tetravalent biotinylated glycodendrimers and bioconjugates measured after 7 days taken from the volume distribution

Sample name	PdI	*d* (V%)/nm	V%
Avidin[a]	0.27	7.9	100
G4-DS-C6B4[a]	0.284	5.6	100
1/0.5	0.164	40.2	100
1/1	0.145	57.1	100
1/1.5	0.201	22.0	100
G4-DS-PEG12B4[a]	0.43	6.1	100
1/0.5	0.155	43.3	100
1/1	0.171	41.5	100
1/1.5	0.241	24.3	100

[a] Samples were only measured after 1 day.

established biohybrid structures appeared broad and had a bimodal behaviour only in the case of **G4-DS-PEG12B4** after 24 h (Fig. 8a and c). After 7 days the dispersity remains entirely stable (compare Tables 2 and 4) but the initial bimodal size distribution also completely disappeared (Fig. 8d; avidin–**G4-DS-PEG12B4** with a molar ratio of 1/1).

Results from Fig. 8 and Table 4 also show that the ratio 1/1 of avidin–**G4-DS-C6B4** induced the formation of large aggregates of diameters up to more than 100 nm and of average diameters of about 50 nm. Compared to that the interaction ratio 1/0.5 of avidin–**G4-DS-PEG12B4** seems to reach aggregates with the highest diameters (∅ 40 nm) which are in the same size range as those obtained by the 1/1 interaction ratio (Fig. 8b and Table 4). Furthermore, applying increasing ratios (1/0.5 and 1/1) for biohybrid structures with **G4-DS-C6B4** one can find increasing diameters for the aggregates. The UV/Vis experiments between **G4-DS-C6B4** and HABA–avidin complexes confirmed the fact of increasing diameters as well since the increasing release of HABA molecules from HABA–avidin complexes was determined (Table ESI-2†). Finally, a surprising tendency is recognizable where the smallest biohybrid structures (∅ ~20 nm) are formed by applying excess of tetravalent **bGD** (Fig. 8). This is also accompanied by the equal/highest release of the azo dye HABA from HABA–avidin complexes in comparison with those with other conjugation ratios (Tables ESI-2 and 3†).

Overall, we cannot postulate "the higher the diameters of biohybrid structures, the higher is the release of HABA molecules from HABA–avidin complexes" as found in the case of the biohybrid structure with bivalent **bGD** (Tables 2 and 3). This point is only observable in the case of **GD-G4-DS-C6B4** up to molar ratio 1/1 against avidin (Table 4, ESI-2 and 3†). In all other conjugation steps similar and excess tetravalent **bGD** with molar ratios of 1/1 and 1/1.5 against avidin result in the same or decreased diameters of the biohybrid structures. This can be explained by the following points, afore-mentioned in the discussion of mono- and bivalent **bGD:** (I) association and dissociation of tetravalent **bGD** on avidin binding sites and/or (II) the fast saturation of the binding pockets of avidin by excess biotin ligands in the conjugation mixture can lead to smaller conjugated avidin–**bGD** structures where dissociation steps are partly favoured. Due to shielding effects of **bGD** and weak binding strengths between avidin and **bGD** one can

assume highly repeating association and dissociation steps in the conjugation of tetravalent **bGD** against avidin that result in the higher release of HABA molecules from the HABA–avidin complexes (Tables ESI-2 and 3†). In such dynamic processes a hampered re-association of the azo dye HABA to the avidin binding site can be supposed.

Theoretical binding calculation models in the future may give answer to be sure about the right number of biotins bound to the avidin macromolecules in the biohybrid structures as summarized in the Tables 2, 4, ESI-2 and ESI-3.† From the experimental point of view using only the HABA displacement assay for assessment gives some limitations for deeper explanation. Moreover, the work by Green *et al.* in the early 1970s gave an indication that in the presence of a higher number of biotin ligands a depolymerisation step, meaning a dissociation process between avidin and biotin ligands, could take place.[45]

Summarizing the results of **G4-DS-C6B4** and **G4-DS-PEG12B4** bioconjugation with avidin, we can state that there is an optimal molar interaction ratio for both types of **bGD** to fabricate monomodal biohybrid structures with large dimensions of up to 100 nm, and **G4-DS-C6B4** exhibits a slightly higher bioconjugation efficiency than **G4-DS-PEG12B4**.

Overall one can conclude the following key factors for fabricating biohybrid structures with avidin as a potential bridging unit and mono-, bi- and tetravalent **bGD** (see also Fig. 9):

(I) In the case of the monovalent **bGD** the **PEG12B** ligand is more efficient than the **C6B** ligand due to its more accessible nature (Table 2). Moreover, the combination of spacer length dependency with sterical demand of **bGD** plays here the deciding role in this specific conjugation case (Fig. 7c). Along with these observations, examples from the literature indicate that dendrons with biotin ligands attached at the focal side may imply a better availability against the binding pockets of avidin to design and fabricate small bioconjugates with avidin as a central unit.[15,26] Despite this it gives no further efforts to evaluate the molar masses of those biohybrid structures.

(II) Bivalent **bGD** fabricate biohybrid structures with diameters up to 30 nm (Table 2), where **G4-DS-C6B2** is more efficient than **G4-DS-PEG12B2**. In this context one would expect larger dimensions of the biohybrid structures that bivalent **bGD** can act as a linear unit against avidin. Due to the randomly distributed biotin ligands, but maximally separated[31] on the surface of the glycodendrimers, it even gives some sterical prevention due to the sterical demand of the **bGD** to undergo the expected biotin–avidin conjugation for this molecular composition. This means that the most efficient spatial arrangement of the two biotin ligands would be 180° on a spherical dendritic PPI scaffold in **G4-DS-C6B2** and **G4-DS-PEG12B2** in order to fabricate biohybrid structures through the polymerization of the bivalent **bGD** and avidin. Moreover this might be also a question of spacer length as Green *et al.* showed in 1971,[45] where the distance between the biotin moieties and hence the length of the hydrophobic linker direct the degree of polymerization of avidin.

(III) Increasing the average number of biotin ligands from 2 up to 4 in **bGD** results in the fabrication of biohybrid structures with dimensions in the range of 20–150 nm (Fig. 8).

(IV) A higher degree of biotin functionalization increases the probability of avidin–biotin conjugation and enables a compensation of the lack of a required spacer length of the **C6B*x*** ($x = 2$ and 4). Surprisingly, this leads in the cases of the bivalent and tetravalent biotinylated GDs **G4-DS-C6B2** and **G4-DS-C6B4** to a slightly higher conjugation efficiency compared to the **PEG12B*x*** ($x = 2$ and 4) and hence to higher sizes of the final biohybrid structures.

Along with this observation it gives a general conjugation behaviour known from the literature that the influence of longer polymer chains on the non-conjugation step between avidin and biotin-end-functionalized PEG chains increases.[37,38] Finally, from our and other studies[15,26,36–38] one can conclude that the structural composition of biotin functionalized (macro-)molecules also plays an important role in the design and fabrication of biotin–avidin conjugates containing supramolecular structures.

(V) The molar interaction ratio is one dominating key factor to tailor the size of the desired biohybrid structures besides the biotin ligand numbers in **bGD**. We could demonstrate that there exists an optimal molar interaction ratio for each component pair for fabricating defined biohybrid structures. The latter conclusion was also drawn from the investigation of the binding of biotin-functionalized liposomes or gold nanoparticles to streptavidin molecules.[52,53]

(VI) To the best of our knowledge, no further dendritic example is presented, where multivalent biotinylated dendrimers or hyperbranched polymers were used to evaluate the fabrication of larger supramolecular structures with defined diameters by using (strept)avidin–biotin conjugation steps in solution as known from other prominent non-covalent conjugation steps such as adamantane-β-cyclodextrin[54,55] or adamantane–azobenzene host–guest interactions on dendritic surfaces.[56]

(VII) Finally, the fabrication of biohybrid structures with different diameters is completely accompanied by intra- and intermolecular association and dissociation processes (Fig. 7) until achieving final diameters. Using specific combination of degree of biotinylation on the glycodendrimer surface (4 biotin ligands) and defined ligand–receptor stoichiometry (1/1 or 1/1.5 molar ratios) dissociation and depolymerisation processes mainly occur that exhibit the same and smaller diameters of the biohybrid structures in contrast to optimal conjugation conditions (Tables 2 and 4).

AF4 study *versus* LILBID MS study on biohybrid structure formation with 1 and 3 equivalents of G4-DS-C6B1

For the estimation of the molar mass distributions of the single components and their associates two different techniques have been applied, the Laser-Induced Liquid Bead Ion/Desorption Mass Spectrometry (LILBID-MS)[57–59] and the Asymmetrical Flow Field Flow Fractionation (AF4).[60–63] Both of them are quite novel methods and their application on biological and biomimetic[64,65] samples have been developed recently.

The molar mass of biohybrid structures formed by the conversion of 1 or 4 equivalents **G4-DS-C6B1** against 1 equivalent

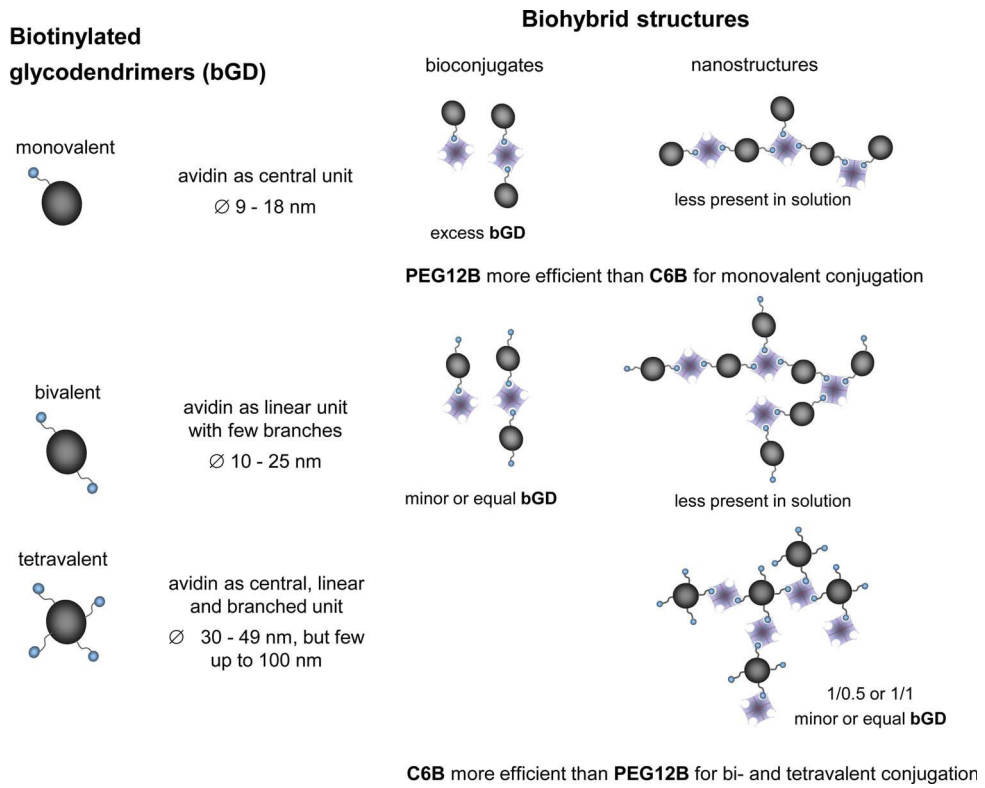

Fig. 9 Summary of the present study for fabricating different nanometer-sized biohybrid structures after 1 day determined by *degree of biotinylation* on the glycodendrimer surface and *defined ligand–receptor stoichiometries*. Short ligand **C6B** or long ligand **PEG12B** on **bGD** were used for avidin–biotin conjugation.

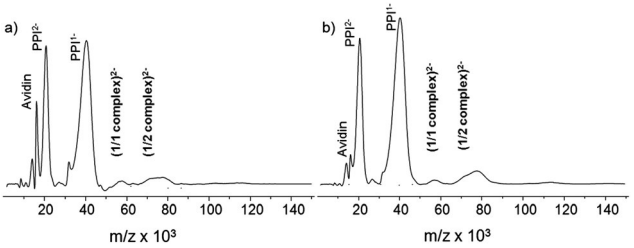

Fig. 10 LILBID-MS spectra of (a) avidin–**G4-DS-C6B1** as 1/1 ratio and (b) avidin–**G4-DS-C6B1** as 1/4 after 24 h.

of avidin was determined by LILBID MS. Fig. 10a shows mainly 1/1 and 1/2 complexes next to free **G4-DS-C6B1** and avidin. This seems reasonable considering the amount of bound **bGD** (Table 3) and the stagnation in sizes as found by the DLS studies (Fig. 5a). However, even a higher amount of **bGD** of 4 equivalents against avidin does not lead to a formation of 1/3 adducts of avidin and **bGD** supporting our explanations to Fig. 7 and also the hypothesis of sterical induced stoichiometry based on the findings of Tomalia *et al.*[66–68]

Additionally, the molar mass distributions of selected bioconjugates were determined by asymmetrical flow field flow fractionation (AF4). In our study the final compositions of the solutions were analysed qualitatively and quantitatively using initial molar ratios of avidin–**G4-DS-C6B1** of 1/1 and 1/3. The AF4 results from avidin–**G4-DS-C6B1** with the molar ratio of 1/1 mainly show free glycodendrimer and free avidin next to the presence of a minor amount of biohybrid structures (Fig. 11a and b and Table 5).

As revealed by the DLS study, there is a lower probability for the glycodendrimer with one **C6B** ligand to undergo the desired avidin–biotin conjugation. The results (Fig. 11c and d and Table 5) from the molar ratio of 1/3 for avidin–**G4-DS-C6B1** revealed, however, the formation of the desired bioconjugates next to few free glycodendrimers. Molar masses of about 170 kDa for the bioconjugates (Table 5) indicate the presence of a 1/2 complex rather than a 1/3 complex. This is in agreement with the LILBID-MS data (Fig. 10b) discussed above.

Molar masses of the single components were determined (Table 6) before studying the fabrication of desired biohybrid structures between **G4-DS-C6B1** and **avidin**. Furthermore, non-biotinylated **G4-DS** was used to optimize the handling of dense shell glycodendrimers in this AF4 study.

Both the molecular and supramolecular structure distributions of the biohybrid structures **G4-DS-C6B1** and avidin were characterized by AF4 (Fig. 11). In the case of the 1/1 ratio of the components we identified free dendrimer, free avidin, the preferred 1/1 bioconjugate and complex nanostructures of them. In the case of the 1/3 ratio, a complete conversion of avidin was identified, while the bioconjugates in 1/2 stoichiometry were mainly determined and not the expected bioconjugates in 1/3 stoichiometry. However, along with the LILBID-MS results a shoulder of the minor 1/1 complex (Fig. 11:

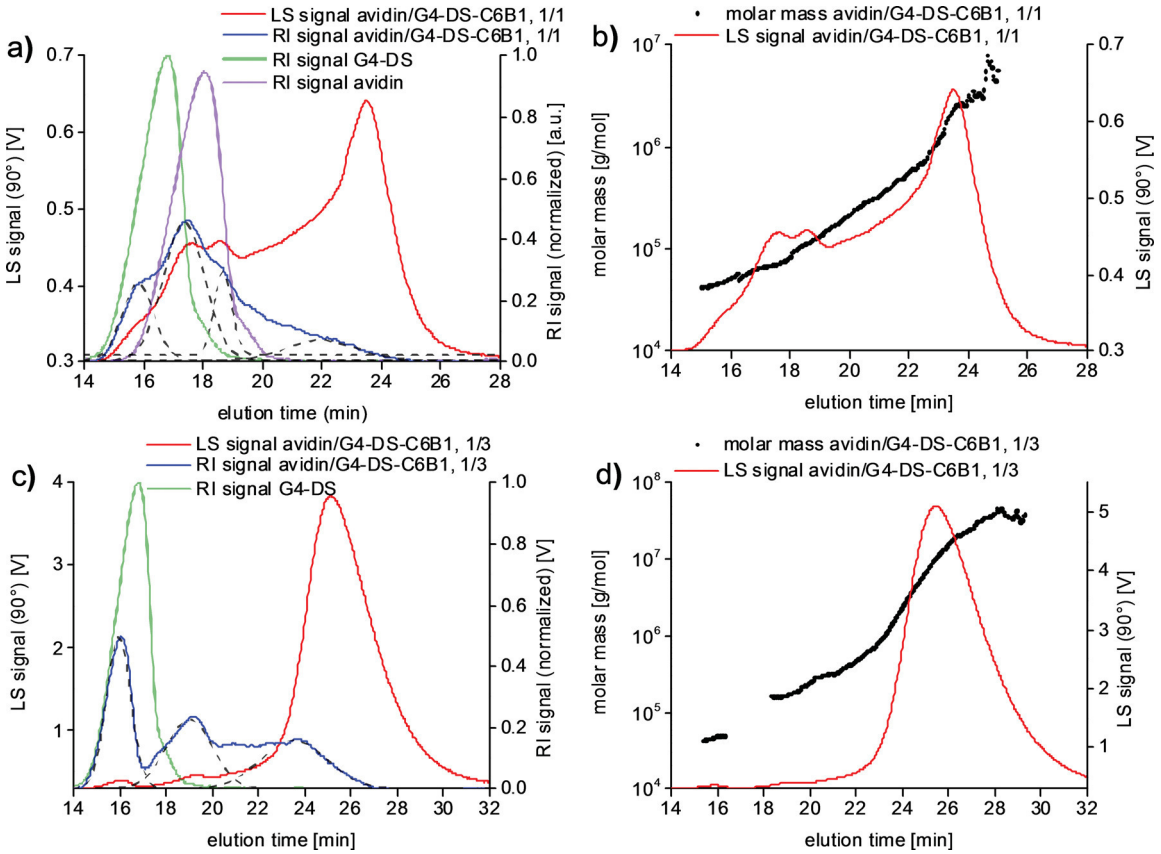

Fig. 11 AF4 results for the conversion of avidin with **G4-DS-C6B1** after 3 days (a) AF4-fractogram with a light scattering (LS) signal and refractive index (RI) signal as a function of elution time, for comparison: RI signal of **G4-DS-C6B1** and avidin; (b) molar mass *vs.* elution time plot for the 1/1 ratio, (c) AF4-fractogram with a light scattering (LS) signal and refractive index (RI) signal as a function of elution time, for comparison: RI signal of **G4-DS-C6B1** and avidin; (d) molar mass *vs.* elution time plot for the 1/3 ratio; the broken lines show the different components found in the superimposed peaks – free **G4-DS** and the conjugate of both **bGD** and avidin.

17–18 min) can be observed but was not analysed to prevent unnecessarily complicated analyses. This is in accordance with the results from DLS, which showed stagnation in sizes for a molar ratio of 1/3. Additionally certain amounts of higher molecular weight associates (denoted as nanostructures) were found. Their appearance in the AF4 fractograms could be a result of the focusing conditions of the separation technique. This effect is the subject of a recent investigation and will be discussed in a forthcoming paper.

In summary AF4 show as well that no complete conversion for 1/1 and 1/3 molar ratios took place where single components (**bGD** and avidin) of the conversion steps were evaluated (Table 5). Despite the fact of hampered avidin–biotin conjugation of the **bGD** to avidin as previously discussed an additional explanation could be the fact that the non-biotinylated glycodendrimer in the **bGD** sample is present in the dendrimer mixture as a result of statistical distribution of the biotin units after the modification of PPI-G4 (Fig. 2). Another point is the decreased conjugation efficiency of the **bGD** due to sterical reasons as discussed above. This effect was also found in the

Table 5 Average molecular weights of the separated components in the bio-hybrid associate avidin–**G4-DS-C6B1** with a molar ratio of 1/1 and 1/3

	M_n [g mol^{-1}]	M_w [g mol^{-1}]	$Đ^a$	Part [%]
Molar ratio of avidin–G4-DS-C6B1 of 1/1				
G4-DS-C6B1	50 100	57 100	1.02	21[b]
Avidin	66 600	67 400	1.01	20[b]
Avidin–**G4-DS-C6B1**	117 000	120 000	1.03	20[b]
Nanostructures	325 000	585 000	1.8	39[b]
Molar ratio of avidin–G4-DS-C6B1 1/3				
G4-DSC6B1	50 100	57 100	1.01	35[c]
Avidin–**G4-DS-C6B1**	169 000	172 000	1.02	23[c]
Nanostructures	729 000	3 930 000	5.4	42[c]

[a] $Đ = M_w/M_n$ represents the percentage of the final composition by a recovery of [b]77% and [c]59%.

Table 6 Average molecular weights of the single components by AF4

	M_n [g mol^{-1}]	M_w [g mol^{-1}]	$Đ^a$	Recovery [%]
Avidin	71 100	77 200	1.09	86
G4-DS	48 000	50 400	1.05	87
G4-DS-C6B1	50 100	57 100	1.14	80
G4-DS-PEG12B1	50 900	52 200	1.02	82

[a] $Đ = M_w/M_n$.

LILBID-MS investigations where signals of the free **bGD** and free avidin are also present in high intensities. The desired conjugates were indeed formed but even a higher molar ratio of 1/3 led only to the formation of 1/2 conjugates of avidin and **G4-DS-C6B1**. This interesting fact could be proven by both methods AF4 and LILBID MS. We also detected next to the desired conjugate nanostructures (Fig. 11) which are characterized by high molar masses and dispersities. Only an excess of multivalent **bGD** to avidin equivalents allows the fabrication of biohybrid structures in a sufficient amount. This implies along with the DLS and TEM results (Fig. 5) that longer biotin ligands (*e.g.* **PEG12B**) or at least two short biotin ligands (**C6B**) attached to the dendritic scaffold are necessary for the efficient formation of the desired biohybrid structures.

Comparing our characterization results with the literature, the characterization of previous supramolecular structures, based on biotin–avidin conjugations and dendritic polymers, is directed to HABA displacement assay, DLS and various chromatography techniques only to identify the presence of successful formation of biohybrid structures. But no further efforts, *e.g.*, by SLS, AF4, or SAXS were undertaken to evaluate the molecular weight, composition and shape of those dendritic supramolecular structures initiated by avidin–biotin conjugation steps.

Experimental

Materials

Sodium tetraborate decahydrate, benzotriazole-1-yl-oxy-tris-(dimethylamino)-phosphonium hexafluorophosphate (**BOP**), dimethylsulfoxide (DMSO), 6-(*N*-biotinylamino)caproic acid (**C6B**), tris(hydroxymethyl)aminomethane (TRIS) and sodium chloride (NaCl) were purchased from Sigma Aldrich. Hydrochloric acid (Tritisol®) was purchased from Merck KGaA. Biotin-PEG_{12}-COOH (**PEG12B**) were obtained from Iris Biotech GmbH. Triethylamine (NEt_3), D-(+)-maltose monohydrate, and borane–pyridine complex (8 M in THF) ($BH_3 \cdot Pyr$) were purchased from Fluka. 4th generation poly(propylene imine) (PPI) dendrimer (DAB Am 64) was supplied by SyMO-Chem (Eindhoven, Netherlands). Avidin was purchased from Life Technologies (Darmstadt, Germany). All chemicals were used as received. All photometric measurements were performed in 1.5–3.0 mL PMMA cuvettes (PLASTIBRAND) from Brand GmbH & Co. KG with a UV/Vis spectrophotometer DU 800 from Beckman Coulter GmbH. A 100 mM TRIS–HCl–0.1 M NaCl solution with pH 7.5 was prepared by dissolving 6.72 g TRIS, 44 mL 1 N HCl and 5.84 g NaCl in 1 L MilliQ water.

Methods

^{1}H NMR spectroscopy. The NMR experiments were performed on a Bruker Avance III 500 NMR spectrometer operating at 500.13 MHz for ^{1}H NMR. DMSO-d_6 or D_2O was used as solvent. The spectra recorded from DMSO-d_6 solutions were calibrated on the solvent signal ($\delta(^1H) = 2.50$ ppm). Spectra recorded from D_2O solutions were referenced on external sodium 3-(trimethylsilyl)-3,3,2,2-tetradeuteropropionate in D_2O ($\delta(^1H) = 0$ ppm).

Infrared spectroscopy. The IR investigations were carried out with a Bruker Vertex 80v spectrometer equipped with a heat able Golden Gate Diamond ATR unit (SPECAC) and an MCT detector. 100 scans of the wavelength range 4000–600 cm^{-1} per measurement were carried out at a spectral resolution of 4 cm^{-1}.

Dynamic light scattering. To characterize the particle size and size distribution, dynamic light scattering (DLS) measurements were carried out at 25 °C at a fixed angle of 173° using the Nano Zetasizer (Malvern), equipped with a He–Ne laser (4 mW) and a digital autocorrelator. The observed data were analyzed very carefully. Thus only measurements with a good fit and an exponential graphic representation were considered here. The particle size distribution was determined using a multimodal peak analysis by intensity, volume and number, respectively. Solutions of the single components and of the biohybrid structures were taken from HABA Displacement Assay.

Matrix-assisted laser desorption/ionization time of flight mass spectrometry (MALDI-TOF MS). The MALDI-TOF experiments were performed on an Autoflex Speed TOF/TOF in a reflector mode and a positive polarity with 2,5-dihydroxybenzoic acid as a matrix.

Laser-induced liquid bead ionization/desorption mass spectrometry (LILBID-MS). LILBID-MS is a recently developed method for the soft mass spectrometric investigation of biomolecules and biomolecular complexes.[57,58] Liquid microdroplets of the aqueous fluid sample (~50 μL) are irradiated by synchronized IR laser pulses ($\lambda = 3$ μm) generated by a home built optical parametric oscillator (OPO) based on a $LiNbO_3$ crystal and pumped by a commercial pulsed Nd-YAG laser. The laser energy is absorbed by O–H stretch vibrations of water molecules, which leads to the superexcitation and subsequent explosive disruption of the droplet. The dendrimers injected into vacuum were analysed by a TOF mass spectrometer. The dendrimer samples (**G4-DS-C6B1**, **G4-DS-C6B2**, **G4-DS-C6B4**, **G4-DS-PEG12B1**, **G4-DS-PEG12B2** and **G4-DS**) were prepared in aqueous solution at concentrations of 4×10^{-6} M. All measurements were performed in anionic mode. LILBID-MS was used to determine the molar masses of compounds **G4-DS-C6B1** and avidin and to study selected bioconjugates of avidin–**G4-DS-C6B1** (5 mM/5 mM and 5 mM/20 mM) in 10 mM TRIS–HCl pH 7.5 after an incubation time of 24 h. The technique is described elsewhere.[57] The experimental requirements of LILBID-MS only allow TRIS–HCl buffer with decreased ionic strength and without additional NaCl in comparison with the buffer used in the DLS study.

UV/Vis spectroscopy. UV/Vis spectra were recorded at room temperature (25 °C) on a Varian Cary 50 UV/Vis spectrometer (Varian Inc.). The slit width was 2 nm.

Spectrophotometric determination of avidin binding sites with 2-(4-hydroxyazobenzene) benzoic acid.[43] The estimation of the avidin binding sites was determined according to the literature[43] by titration experiments of avidin with a starting concentration $c_o = 10.1$ μM with a solution of the azo dye HABA (2-(4-hydroxyazobenzene) benzoic acid) with a concentration $c_t = 0.3$ mM. The avidin solution was titrated with appropriate amounts of a concentrated biotinylated macromolecule

solution in 0.1 M TRIS–HCl buffer with 0.1 M NaCl at pH 7.4. At the end of the titration, the titrated solution was diluted by approximately 70% of the starting volume. The resulting spectrum for each titration step was corrected by the appropriate dilution factor. Every titration experiment revealed the specific activity of avidin as specified by the supplier.

HABA displacement titrations – spectrophotometric determination of avidin binding capacity with biotin and its analogs.[43] The titration experiments of the HABA–avidin complex were carried out with biotin (c_t = 0.185 mM), **G4-DS** (c_t = 0.15 mM), **G4-DS-C6B1** (c_t = 0.15 mM), **G4-DS-C6B2** (c_t = 0.15 mM), **G4-DS-C6B4** (c_t = 0.15 mM), **G4-DS-PEG12B1** (c_t = 0.15 mM), **G4-DS-PEG12B2** (c_t = 0.15 mM) and **G4-DS-PEG12B4** (c_t = 0.15 mM) in a 3-fold determination in disposable sizing UV microcuvettes. Therefore the solution (HABA–avidin complex; c_{avidin} = 10.1 μM and $c_{HABA} = 16 \times c_{avidin}$ to ensure fast saturation of the avidin binding sites by the azo dye HABA) was titrated with appropriate amounts of a concentrated biotinylated macromolecule solution in 0.1 M TRIS–HCl buffer with 0.1 M NaCl at pH 7.4. At the end of the titration, the titrated solution was diluted by approximately 70% of the starting volume. The resulting spectrum for each titration step was corrected by the appropriate dilution factor. This procedure was also used to determine the degree of biotin ligand functionalization through regression of the two linear regions of the curves before and after the equivalence point (Fig. 4).

HABA displacement assay for UV/Vis observation of the formation processes for the different biohybrid structures. A HABA–avidin solution with an avidin concentration of 1 mg mL^{-1} was prepared with a 16-fold excess of HABA to avidin. This solution was converted with a biotinylated compound. The final avidin concentration was 6.25 μM within all samples. The resulting bioconjugates were measured by UV/Vis spectroscopy after 24 h. The dynamic light scattering measurements were carried out after 1 or as indicated in the main part 7 days.

Determination of bound biotinylated glycodendrimer to avidin. To determine the apparent amount of coupled biotinylated glycodendrimer to avidin the measured absorbance values at 500 nm of the avidin–biotinylated glycodendrimer mixtures and the linear regression of the lower part of the titration curves were used to calculate the related amount of biotinylated glycodendrimer coupled to avidin.

Asymmetrical flow field flow fractionation. The AF4 instrument was an Eclipse 3 Separation System (Wyatt Technology Europe, Germany). The flow was controlled with an isocratic pump (1200 Series from Agilent Technologies, USA) and all injections were performed with an autosampler (1200 Series from Agilent Technologies, USA). A long AF4-channel (Wyatt Technology Europe, Germany) having a tip-to-tip length of 26.65 cm and a nominal thickness of 490 μm was used. The ultra-filtration membrane forming the accumulation wall was made of regenerated cellulose with a molecular weight cut off of 10 kDa (Wyatt Technology Europe, Germany). The detection system consists of a multi-angle laser light scattering detector (DAWN EOS from Wyatt Technology Europe, Germany) operating at a wavelength of 690 nm and a refractive index detector (Dn 2010 from WGE Dr Bures, Germany) operating at a wavelength of 620 nm. Carrier liquid was prepared with 0.1 M TRIS–HCl (Sigma-Aldrich, Germany), 0.1 M NaCl (Carl Roth, Germany) and 0.02% (w/v) NaN_3 (Carl Roth, Germany) dissolved in pure water, which was deionised, UV treated and ultra-filtered using Purelab Plus UV/UF equipment (ELGA LabWater, Germany).

The sample injection of 100 μL into the channel was performed at a flow rate of 0.2 mL min^{-1} for 2 min. The sample load was approximately 100–150 μg. Separation and determination of the molecular weight of the sample were performed after focusing at 3 mL min^{-1} over a period of 2 min and elution with a linearly decaying cross flow from 3 mL min^{-1} to 0 mL min^{-1} in 15 min and afterwards without any cross flow for 10 min. The detector flow rate was constant at 1 mL min^{-1} throughout the measurement. Two measurements of each sample were carried out. Afterwards a blank run was performed for the baseline subtraction of the pressure sensitive signal of the refractive index detector.

Collecting and processing of detector data were made by the Astra software, version 5.3.4.20 (Wyatt Technology, USA). The molar mass dependence of the elution volume was fitted with 4th degree exponential. For M_w determination the dn/dc values were externally determined at 25 °C using the refractive index detector of the system. The refractive index increments, dn/dc of 0.174 mL g^{-1} for avidin, 0.149 mL g^{-1} for **G4-DS**, 0.159 mL g^{-1} for **G4-DS-C6B1**, 0.162 mL g^{-1} for **G4-DS-C6B1**, and 0.160 mL g^{-1} for the avidin–**G4-DS-C6B1** associates (at different molar ratios), were determined for the light scattering calculations.

Transmission electron microscopy. The morphology and size of the particles were determined by transmission electron microscopy with the Libra 120 (Carl Zeiss AG, Oberkochen, Germany) along with the dynamic light scattering measurements. Samples were prepared by dropping sample solutions with an increased concentration of 2 mg mL^{-1} and a decreased molarity of the buffer (10 mM) on carbon coated gold grids. The air dried samples were examined in the transmission electron microscope at an acceleration voltage of 120 kV.

Purification of conjugation solution with G4-DS-PEG12B2 with 1/1 molar ratio. 5.4 mL of an equimolar solution of G4-DS-PEG12B2 and avidin (2.19×10^{-5} M) in TRIS–HCl–NaCl 0.1 M was equilibrated for 24 h. The resulting solution was diluted up to approximately 35 mL and subsequently filtered with a mPES membrane of 300 kDa for up to 100 mL with an approximate pressure of 200 mbar and a volume flow of 15 mL s^{-1}. Every 20 mL of the sample obtained by the filtration procedure was taken for DLS measurements. The hollow fibre filtration method was done by using the KrosFlo-Research-IIi (SpectrumLabs, USA), equipped with a polysulfone-based separation module (MWCO: 300 kDa, SpectrumLabs, USA).

Synthesis of compounds

General procedure for the synthesis of the precursor G4-C6B*x*, G4-PEG12B*x*, *x* = 1, 2 and 4. 4th generation PPI dendrimer (**G4**, 7168 g mol^{-1}; *considering footnote i in paper*), 6-(*N*-biotinylamino)caproic acid (**C6B**, 357.47 g mol^{-1}) or biotin-PEG_{12}-COOH (**PEG12B**, 844.0 g mol^{-1}), benzotriazole-1-yl-oxy-tris-(dimethylamino)-phosphonium hexafluorophosphate (**BOP**,

Table 7 Molar ratio and molecular weight of the educts for the precursor synthesis

Precursor	**G4**, eq. [mol] [mg]	**C6B**, eq. [mol] [mg]	**PEG12B**, eq. [mol] [mg]	**BOP**, eq. [mol] [mg]	**NEt_3**, eq. [mol] [mL]
G4-C6B1	1.0	1.1	—	2.5	10.0
	1.395×10^{-5}	1.535×10^{-5}		3.488×10^{-5}	1.395×10^{-4}
	100.0	5.5		15.5	0.019
G4-C6B2	1.0	2.2	—	5.0	20.0
	1.395×10^{-5}	1.535×10^{-5}		6.975×10^{-5}	2.790×10^{-4}
	100.0	11.0		31.0	0.038
G4-C6B4	1.0	4.4	—	11.0	20.0
	1.395×10^{-5}	1.535×10^{-5}		16.89×10^{-5}	2.790×10^{-4}
	100.0	22.0		62.0	0.038
G4-PEG12B1	1.0	—	1.1	5.0	10.0
	1.395×10^{-5}		1.535×10^{-5}	6.975×10^{-5}	1.395×10^{-4}
	100.0		13.0	31.0	0.019
G4-PEG12B2	1.0	—	2.2	10.0	20.0
	1.395×10^{-5}		1.535×10^{-5}	13.95×10^{-5}	2.790×10^{-4}
	100.0		26.0	62.0	0.038
G4-PEG12B4	1.0	—	4.4	8.8	20.0
	1.395×10^{-5}		3.07×10^{-5}	13.95×10^{-5}	2.790×10^{-4}
	100.0		52.0	54.6	0.038

442.28 g mol^{-1}) and triethylamine (**Et_3N**, 0.73 g mL^{-1}, 101.19 g mol^{-1}) were taken up in DMSO (10 mL). The solution was stirred at room temperature for 2 days. The crude product was purified by dialysis in deionized water for 2 days. A yellowish viscous substance was obtained by freeze drying. The product was yielded quantitatively as a solid. The molar ratios for both conversion steps are summarized in Table 7 and Table 8, respectively.

G4-C6Bx *or* ***G4-PEG12Bx****, x = 1, 2 or 4.*

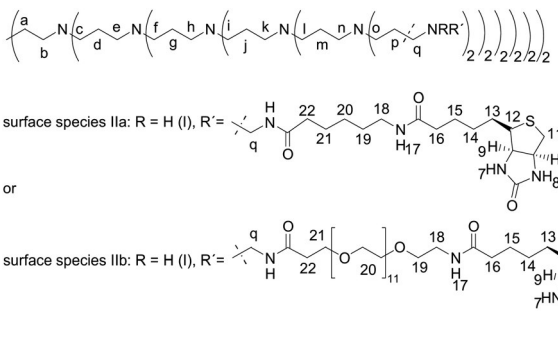

G4-C6Bx *(x = 1, 2 or 4).* ^{1}H NMR (D_2O): 4.60 (10), 4.41 (9), 3.32 (12), 3.2–2.3 (18, *b,c,e,f,h,I,k,l,n,o,q* of IIb), 2.89 (*q* of I), 2.99 and 2.78 (11), 2.24 (16,22), 1.9–1.6 (1H of 13,*a,d,g,j,m,p*), 1.6–1.25 ppm (1H of 13,14,15,19-21). Free ligand (–COOH): 1.55 (21), 2.17 (22) (Fig. ESI-1†); IR: 3298 (NH_2), 2865 (CH, CH_2), 2802 (CH, CH_2), 1646 (C═O), 1566 (N–H, NH_2), 1384 (CH_2, CH_3) 1009 cm^{-1} (C–O).

G4-PEG12Bx *(x = 1, 2 or 4).* ^{1}H NMR (D_2O): 4.60 (10), 4.41 (9), 3.77 (21), 3.69 (20), 3.62 (19), 3.38 (18), 3.33 (12), 3.3–2.3 (*b,c,e,f,h,I,k,l,n,o,q* of IIb), 2.93 (*q* of I), 2.99 and 2.78 (11), 2.52 (22), 2.27 (16), 1.9–1.6 (1H of 13, *a,d,g,j,m,p*), 1.6–1.35 ppm (1H of 13,14,15) (Fig. 3a). Free ligand (–COOH): 3.73 (21), 2.45 (22) (Fig. 3a); IR: 3305 (NH_2), 2870 (CH, CH_2), 2802 (CH, CH_2), 1646 (C═O), 1566 (N–H, NH_2), 1384 (CH_2, CH_3) 1010 cm^{-1} (C–O).

General procedure for the synthesis of the maltose modified dense shell glycodendrimers. The precursor, maltose monohydrate (360.31 g mol^{-1}) and borane–pyridine complex (BH_3 × Pyr, 8 M) were taken up in a sodium borate buffer (25 mL, 0.1 M). The solution was stirred at 50 °C for 7 days. The crude product was purified twice by dialysis with deionized water for 4 days to ensure the capture of impurities. The solid product was obtained by freeze drying. The molar ratios and yields for the conversion steps are summarized in Table 8.

G4-DS*.*

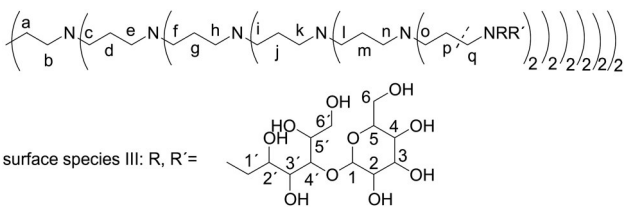

^{1}H NMR: (D_2O). Signal assignment according to B. Klajnert and D. Appelhans *et al.*, *Chem. Eur. J.*, 2008, **14**, 7030–7041.[41]

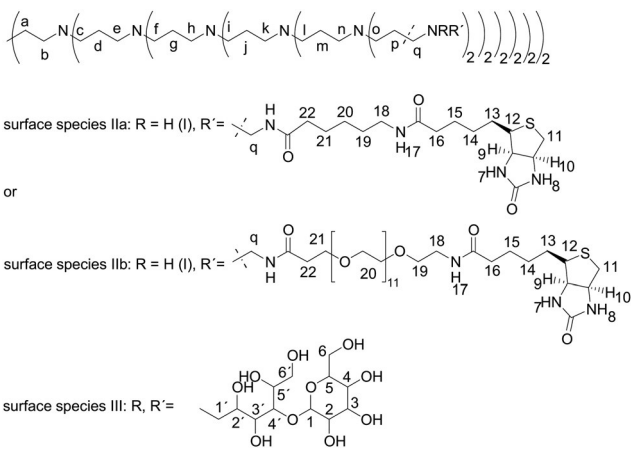

G4-DS-C6Bx *(x = 1, 2 or 4).* ^{1}H NMR (D_2O): 5.4–5.0 (1), 4.60 (10), 4.43 (9), 4.4–3.3 (2-6,2′-6′,12), 3.3–2.2 (1′,11,16,18,22,*b,c,e,f,h,I,k,l,n,o,q*), 2.2–1.1 ppm (13-15,19-21,*a,d,g,j,m,p*) (Fig. ESI-2†); IR: 3298 (NH_2), 2865 (CH, CH_2),

Table 8 Molar ratio and molecular weight of the precursors for the glycodendrimer synthesis and overall yield

Glycodendrimer	Precursor, M_n, eq. [mol] [mg]		Maltose, eq. [mol] [mg]	$BH_3 \times Pyr$, eq. [mol] [mL]	Yield, [%]
G4-DS	G4, 7168 g mol^{-1}	1.0	1280.0	1280.0	94
		1.395×10^{-5}	17.86×10^{-3}	17.86×10^{-3}	
		100.0	6.44	2.24	
G4-DS-C6B1	G4-C6B1, 7500 g mol^{-1}	1.0	1280.0	1280.0	95
		1.379×10^{-5}	17.65×10^{-3}	17.65×10^{-3}	
		105.0	6.36	2.22	
G4-DS-C6B2	G4-C6B2, 7850 g mol^{-1}	1.0	1280.0	1280.0	92
		1.388×10^{-5}	17.77×10^{-3}	17.77×10^{-3}	
		109.0	6.40	2.24	
G4-DS-C6B4	G4-C6B4, 8500 g mol^{-1}	1.0	1280.0	1280.0	96
		1.282×10^{-5}	16.41×10^{-3}	16.41×10^{-3}	
		109.0	5.91	2.07	
G4-DS-PEG12B1	G4-PEG12B1, 8000 g mol^{-1}	1.0	1280.0	1280.0	93
		1.377×10^{-5}	17.63×10^{-3}	17.63×10^{-3}	
		110.2	6.35	2.22	
G4-DS-PEG12B2	G4-PEG12B2, 8820 g mol^{-1}	1.0	1280.0	1280.0	95
		1.385×10^{-5}	17.73×10^{-3}	17.73×10^{-3}	
		122.2	6.39	2.23	
G4-DS-PEG12B4	G4-PEG12B4, 10 500 g mol^{-1}	1.0	1280.0	1280.0	92
		0.842×10^{-5}	10.78×10^{-3}	10.78×10^{-3}	
		88.4	6.39	1.36	

2802 (CH, CH_2), 1646 (C═O), 1566 (N–H, NH_2), 1384 (CH_2, CH_3) 1009 cm^{-1} (C–O); LILBID MS: ***G4-DS-C6B1*** (45 900 g mol^{-1} 118 maltose units and 1 C6B moiety connected to PPI-G4); m/z = top of the peak of about 46 000 (M^-) (Fig. ESI-4b†). The number of maltose units in **G4-DS-C6B1** was calculated by LILBID MS and confirmed from the ^1H NMR spectrum recorded in D_2O taking into account the degree of biotin functionalization determined through HABA displacement titrations (Fig. 4 and Table 1). ***G4-DS-C6B2***: m/z = 46 100 (M^-) (Fig. ESI-5a†), ***G4-DS-C6B4***: m/z = 47 650 g mol^{-1} (M^-) (Fig. ESI-6b†).

G4-DS-PEG12Bx *(x = 1, 2 or 4).* ^1H NMR (D_2O): 5.4–5.0 (1), 4.60 (10), 4.43 (9), 4.4–3.3 (2-6,2′-6′,12,18,19,21), 3.70 (20), 3.3–2.2 (1′,11,12,16,22,*b*,*c*,*e*,*f*,*h*,*I*,*k*,*l*,*n*,*o*,*q*), 2,27 (16), 2.2–1.1 (13-15,*a*,*d*,*g*,*j*,*m*,*p*) (Fig. 3b); IR: 3305 (NH_2), 2870 (CH, CH_2), 2802 (CH, CH_2), 1646 (C═O), 1566 (N–H, NH_2), 1384 (CH_2, CH_3) 1010 (C–O); LILBID MS: ***G4-DS-PEG12B1*** m/z = 45 900 (M^-) (Fig. ESI-5b†). ***G4-DS-PEG12B2***: m/z = 45 700 (M^-) (Fig. ESI-6a†); ***G4-DS-PEG12B4***: M = 43 750 g mol^{-1} (determined by ^1H NMR approach[41]).

Conclusion

We have demonstrated the successful fabrication of biohybrid structures tailored by non-covalent interactions. Using avidin–biotin conjugation as the deciding non-covalent interaction step, different nanometer-sized biohybrid structures can be established by using different molar interaction ratios between mono-, bi- and tetravalent biotinylated glycodendrimers (**bGD**) and avidin, shortly summarized in Fig. 9. Furthermore, these biohybrid structures were comprehensively analysed by different complementary methods such as DLS, UV/Vis and TEM. Moreover LILBID-MS and AF4 investigations for first defined molar interaction ratios (1/1 and 3/1) between monovalent **bGD** with the short **C6B** ligand and avidin gave interesting new insights, that at least two key factors (*type of biotinylation* and *higher ligand–receptor stoichiometries*) are really important in the formation of desired biohybrid structures by inducing the necessary avidin–biotin conjugations.

This study clearly emphasized how the size dimension of the biohybrid structures can be controlled by different key factors. Controlling the maximal size dimensions of the biohybrid structures up to 100 nm is given by the interplay of two key factors: *degree of biotinylation* on the dendritic glycosurface needs 4 biotin ligands, and *defined ligand–receptor stoichiometries*, even more preferring minor or equimolar **bGD**.

Moreover, the *quality of biotin ligand functionalization* (*e.g.* length and chemical nature of the spacer or the number of coupled biotin ligands) *on the dendritic glycosurface* is a pivotal aspect in the fine-tuning in order to fabricate biohybrid nanostructures with tailored characteristics. Preferentially establishing avidin as a central unit in the nanostructures, the *longer **PEG12B** ligand in monovalent **bGD*** proved to be the more effective in the bioconjugation strategy than the *shorter C6B ligand*.

Overall the fabrication of (complex) biohybrid structures by a simultaneous approach is possible. Here, the *defined ligand–receptor stoichiometries* give us the possibility to tune the size dimensions of the biohybrid structures (<20, <30 or up to 100 nm). This study further implies that a higher number of biotin ligands (>4 biotin ligands) in glycodendrimer macromolecules in the biohybrid structure fabrication approach will immediately result in stronger aggregation and/or depolymerisation steps depending on the use of *ligand–receptor stoichiometry*. Generally, the fabrication of biohybrid structures is tailored by inter- and intramolecular association and dissociation steps until final sizes of the supramolecular structures are achieved.

However, the next challenge will be the integration of separation methods (dialysis, hollow fiber filtration or AF4) to separate non-biotinylated and non-conjugated macromolecules or smaller hybrid structures from larger supramolecular structures in a more intense fashion as a next step for the preparation of more defined biohybrid structures for biomedical applications.

Acknowledgements

This work was funded by the Saxon Ministry for Science and Art and the German Ministry for Education and Science. The authors thank Dr Sahre for carrying out MALDI-TOF mass spectrometry experiments, Mr Philipp Fenner for performing the HFF purification and accompanied DLS measurements, Mrs Linda Scharfenberg for performing one part of the AF4 measurements and Dr J. Hoffmann for supporting LILBID-MS experiments. The work was also done in the COST Action TD0802 "Dendrimers in biomedical applications".

References

1 J. A. Barreto, W. O'Malley, M. Kubeil, B. Graham, H. Stephan and L. Spiccia, *Adv. Mater.*, 2011, **23**, H18–H40.
2 H. G. Börner, *Prog. Polym. Sci.*, 2009, **34**, 811–851.
3 W.-D. Jang, K. M. Kamruzzaman Selim, C.-H. Lee and I.-K. Kang, *Prog. Polym. Sci.*, 2009, **34**, 1–23.
4 Y. Liu, M. Solomon and S. Achilefu, *Med. Res. Rev.*, 2010, 3–32.
5 D. Q. McNerny, P. R. Leroueil and J. R. Baker, *WIREs Nanomedicine and Nanobiotechnology*, 2010, **2**, 249–259.
6 K. E. Sapsford, K. M. Tyner, B. J. Dair, J. R. Deschamps and I. L. Medintz, *Anal. Chem.*, 2011, **83**, 4453–4488.
7 M.-M. Seale-Goldsmith and J. F. Leary, *WIREs Nanomedicine and Nanobiotechnology*, 2009, **1**, 553–567.
8 K. E. Sapsford, W. R. Algar, L. Berti, K. B. Gemmill, B. J. Casey, E. Oh, M. H. Stewart and I. L. Medintz, *Chem. Rev.*, 2013, **113**, 1904–2074.
9 N. M. Green, *Biochem. J.*, 1963, **89**, 599–609.
10 W. Zhu, B. Okollie, Z. M. Bhujwalla and D. Artemov, *Magn. Reson. Med.*, 2008, **59**, 679–685.
11 H. C. Yoon, M.-Y. Hong and H.-S. Kim, *Anal. Biochem.*, 2000, **282**, 121–128.
12 M. Yang, E. M. W. Tsang, Y. A. Wang, X. Peng and H.-Z. Yu, *Langmuir*, 2005, **21**, 1858–1865.
13 H. Xu, C. A. S. Regino, Y. Koyama, Y. Hama, A. J. Gunn, M. Bernardo, H. Kobayashi, P. L. Choyke and M. W. Brechbiel, *Bioconjugate Chem.*, 2007, **18**, 1474–1482.
14 S. Theoharis, U. Krueger, P. H. Tan, D. O. Haskard, M. Weber and A. J. T. George, *J. Immunol. Methods*, 2009, **343**, 79–90.
15 L. Tao, J. Geng, G. Chen, Y. Xu, V. Ladmiral, G. Mantovani and D. M. Haddleton, *Chem. Commun.*, 2007, 3441–3443.
16 S. Sofou, *Int. J. Nanomed.*, 2008, **3**, 181–199.
17 M.-Y. Hong, D. Lee, H. C. Yoon and H.-S. Kim, *Bull. Korean Chem. Soc.*, 2003, **24**, 1197.
18 H. L. J. Malý, A. Semerádtová, M. Štofik and L. Kováčik, *Nanotechnology*, 2009, **20**, 385101.
19 M. Gaumet, A. Vargas, R. Gurny and F. Delie, *Eur. J. Pharm. Biopharm.*, 2008, **69**, 1–9.
20 S. Lindegren, B. Karlsson, L. Jacobsson, H. Andersson, R. Hultborn and G. Skarnemark, *Clin. Cancer Res.*, 2003, **9**, 3873s–3879s.
21 S. Lindegren, H. Andersson, L. Jacobsson, T. Bäck, G. Skarnemark and B. Karlsson, *Bioconjugate Chem.*, 2002, **13**, 502–509.
22 Z. Yao, M. Zhang, H. Sakahara, T. Saga, Y. Arano and J. Konishi, *J. Natl. Cancer Inst.*, 1998, **90**, 25–29.
23 Z. Yao, M. Zhang, H. Sakahara, T. Saga, Y. Nakamoto, N. Sato, S. Zhao, Y. Arano and J. Konishi, *Ann. Nucl. Med.*, 1998, **12**, 115–118.
24 R. Lotan and A. Raz, *Ann. N. Y. Acad. Sci.*, 1988, **551**, 385–398.
25 Y. Hama, Y. Urano, Y. Koyama, M. Kamiya, M. Bernardo, R. Paik, M. C. Krishna, P. L. Choyke and H. Kobayashi, *Neoplasia*, 2006, **8**, 607–612.
26 D. Y. Wah, J. Fahrer, Y. Wu, K. Eisele, S. L. Kuan, H. Barth and T. Weil, *Adv. Healthcare Mater.*, 2013, 1–10.
27 F. Petronzelli, A. Pelliccia, A. M. Anastasi, R. Lindstedt, S. Manganello, L. E. Ferrari, C. Albertoni, B. Leoni, A. Rosi, V. D'Alessio, K. Deiana, G. Paganelli and R. De Santis, *Cancer Biother. Radiopharm.*, 2010, **25**, 563–570.
28 S. Svenson, in *Kirk-Othmer Encyclopedia of Chemical Technology*, John Wiley & Sons, Inc., 2000.
29 A. R. Menjoge, R. M. Kannan and D. A. Tomalia, *Drug Discovery Today*, 2010, **15**, 171–185.
30 M. R. Longmire, M. Ogawa, P. L. Choyke and H. Kobayashi, *Bioconjugate Chem.*, 2011, **22**, 993–1000.
31 H. J. Han, K. B. Sebby, D. J. Singel and M. J. Cloninger, *Macromolecules*, 2007, **40**, 3030–3033.
32 L. E. Samuelson, K. B. Sebby, E. D. Walter, D. J. Singel and M. J. Cloninger, *Org. Biomol. Chem.*, 2004, **2**, 3075–3079.
33 K. B. Sebby, E. D. Walter, R. J. Usselman, M. J. Cloninger and D. J. Singel, *J. Phys. Chem. B*, 2011, **115**, 4613–4620.
34 E. D. Walter, K. B. Sebby, R. J. Usselman, D. J. Singel and M. J. Cloninger, *J. Phys. Chem. B*, 2005, **109**, 21532–21538.
35 S. Hou, X.-L. Sun, C.-M. Dong and E. L. Chaikof, *Bioconjugate Chem.*, 2004, **15**, 954–959.
36 K. Kaiser, M. Marek, T. Haselgrübler, H. Schindler and H. J. Gruber, *Bioconjugate Chem.*, 1997, **8**, 545–551.
37 S. Ke, J. C. Wright and G. S. Kwon, *Bioconjugate Chem.*, 2007, **18**, 2109–2114.
38 S. Ke, J. C. Wright and G. S. Kwon, *Bioconjugate Chem.*, 2007, **18**, 1644–1650.
39 S. Venkataraman, J. L. Hedrick, Z. Y. Ong, C. Yang, P. L. R. Ee, P. T. Hammond and Y. Y. Yang, *Adv. Drug Delivery Rev.*, 2011, **63**, 1228–1246.
40 B. Ziemba, A. Janaszewska, K. Ciepluch, M. Krotewicz, W. A. Fogel, D. Appelhans, B. Voit, M. Bryszewska and B. Klajnert, *J. Biomed. Mater. Res., Part A*, 2011, **99**, 261–268.
41 B. Klajnert, D. Appelhans, H. Komber, N. Morgner, S. Schwarz, S. Richter, B. Brutschy, M. Ionov, A. K. Tonkikh, M. Bryszewska and B. Voit, *Chem.–Eur. J.*, 2008, **14**, 7030–7041.

42 D. A. Tomalia and M. Rookmaker, in *Polymer Data Handbook*, ed. J. E. Mark, Oxford University Press, New York, 2nd edn, 2009, pp. 979–982.
43 N. M. Green, in *Methods in Enzymology*, ed. B. M. Donald and D. W. Lemuel, Academic Press, 1970, vol. 18, Part A, pp. 418–424.
44 G. Houen and K. Hansen, *J. Immunol. Methods*, 1997, **210**, 115–123.
45 N. M. Green, *Biochem. J.*, 1971, **125**, 781–791.
46 J. Bloustine, T. Virmani, G. M. Thurston and S. Fraden, *Phys. Rev. Lett.*, 2006, **96**, 087803.
47 J. Wu, Z. Wang, W. Lin and S. Chen, *Acta Biomater.*, 2013, **9**, 6414–6420.
48 N. Ngadi, J. Abrahamson, C. Fee and K. Morison, *Int. J. Biol. Life Sci.*, 2009, **5**, 106–110.
49 R. Kelsall, I. W. Hamley and M. Geoghegan, *Nanoscale Science and Technology*, Wiley, 2005.
50 B. K. Sinha and C. F. Chignell, in *Methods in Enzymology*, ed. L. D. W. Donald and B. McCormick, Academic Press, 1979, vol. 62, pp. 295–308.
51 L. Pugliese, A. Coda, M. Malcovati and M. Bolognesi, *J. Mol. Biol.*, 1993, **231**, 698–710.
52 E. T. Kisak, M. T. Kennedy, D. Trommeshauser and J. A. Zasadzinski, *Langmuir*, 2000, **16**, 2825–2831.
53 S. Connolly, S. Cobbe and D. Fitzmaurice, *J. Phys. Chem. B*, 2001, **105**, 2222–2226.
54 I. Böhm, K. Isenbügel, H. Ritter, R. Branscheid and U. Kolb, *Angew. Chem., Int. Ed.*, 2011, **50**, 7896–7899.
55 H. Wang, S. Wang, H. Su, K.-J. Chen, A. L. Armijo, W.-Y. Lin, Y. Wang, J. Sun, K.-I. Kamei, J. Czernin, C. G. Radu and H.-R. Tseng, *Angew. Chem., Int. Ed.*, 2009, **48**, 4344–4348.
56 H. Jin, Y. Zheng, Y. Liu, H. Cheng, Y. Zhou and D. Yan, *Angew. Chem., Int. Ed.*, 2011, **50**, 10352–10356.
57 N. Morgner, H. Barth and B. Brutschy, *Aust. J. Chem.*, 2006, **59**, 109–114.
58 N. Morgner, T. Kleinschroth, H.-D. Barth, B. Ludwig and B. Brutschy, *J. Am. Soc. Mass Spectrom.*, 2007, **18**, 1429–1438.
59 L. Sokolova, I. Wittig, H.-D. Barth, H. Schägger, B. Brutschy and U. Brandt, *Proteomics*, 2010, **10**, 1401–1407.
60 F. A. Messaud, R. D. Sanderson, J. R. Runyon, T. Otte, H. Pasch and S. K. R. Williams, *Prog. Polym. Sci.*, 2009, **34**, 351–368.
61 L. Nilsson, *Food Hydrocolloids*, 2013, **30**, 1–11.
62 B. Roda, A. Zattoni, P. Reschiglian, M. H. Moon, M. Mirasoli, E. Michelini and A. Roda, *Anal. Chim. Acta*, 2009, **635**, 132–143.
63 M. Raviña, M. de la Fuente, J. Correa, A. Sousa-Herves, J. Pinto, E. Fernandez-Megia, R. Riguera, A. Sanchez and M. J. Alonso, *Macromolecules*, 2010, **43**, 6953–6961.
64 S. Boye, N. Polikarpov, D. Appelhans and A. Lederer, *J. Chromatogr., A*, 2010, **1217**, 4818–4849.
65 S. Boye, D. Appelhans, V. Boyko, S. Zschoche, H. Komber, P. Friedel, P. Formanek, A. Janke, B. Voit and A. Lederer, *Biomacromolecules*, 2012, **13**, 4222–4235.
66 D. A. Tomalia, *Prog. Polym. Sci.*, 2005, **30**, 294–324.
67 D. A. Tomalia, *J. Nanopart. Res.*, 2009, **11**, 1251–1310.
68 D. A. Tomalia, *Soft Matter*, 2010, **6**, 456–474.